# A Low-Cost Method for Optical Tomography

**Mohsen Erfanzadeh, Saied Alikhani, Mohammad Ali Ansari, Ezeddin Mohajerani**

Laser and Plasma Research Institute, Shahid Beheshti University.G.C., Tehran, Iran.

**Abstract:**

**Introduction:** In this study, arrangement of a low-cost optical tomography device compared to other methods such as frequency domain diffuse tomography or time domain diffuse tomography is reported. This low-cost diffuse optical imaging technique is based on the detection of light after propagation in tissue. These detected signals are applied to predict the location of in-homogeneities inside phantoms. The device is assessed for phantoms representing homogenous healthy breast tissues as well as those representing healthy breast tissues with a lesion inside.

**Methods:** A diode laser at 780nm and 50 mW is used as the light source. The scattered light is then collected from the outer surface of the phantom by a detector. Both laser and detector are fiber coupled. The detector fiber may turn around the phantom to collect light scattered at different angles. Phantoms made of intralipid as the scattering medium and ink as the absorbing medium are used as samples. Light is collected after propagation in the phantoms and the capability of the device in collecting data and detecting lesions inside the phantoms is assessed. The fact that the detection fiber orbits around the sample and detects light from various angles has eliminated the need to use several detectors and optical fibers. The results obtained from experiments are compared with the results obtained from a finite element method (FEM) solution of diffusion equation in cylindrical geometry written in FORTRAN.

**Results:** The graphs obtained experimentally and numerically are in good accordance with each other. The device has been able to detect lesions up to 13 mm inside the biological phantom.

**Conclusion:** The data achieved by the optical tomography device is compared with the data achieved via a FEM code written in FORTRAN. The results indicate that the presented device is capable of providing the correct pattern of diffusely backscattered and transmitted light. The data achieved from the device is in excellent correlation with the numerical solution of the diffusion equation. Therefore, results indicate the applicability of the reported device. This device may be used as a base for an optical imaging. It is also capable of detecting lesions inside the phantoms.

**Keywords:** optical tomography; diode laser; biological phantom.

## Introduction

Statistics reveal that the lung, bronchus, and breast in women are the commonest cancers and are reported to have caused the majority of cancer related deaths (1). Furthermore, breast cancer is posing serious threat to women's health (2). Nevertheless, if detected early and treated with appropriate therapy, its mortality can be decreased (3). Therefore, screening women for detection of breast cancer is considered to be of

great importance. One of the commonest methods for breast lesion detection is X-ray mammography. However, it is shown that its success is hampered by a number of drawbacks. For instance, trustworthiness of X-ray mammography is hindered by false positives and negatives results (4-5). Furthermore, its ionizing radiation might be harmful to the patient (6). Consequently, alternative diagnostic techniques such as magnetic resonance imaging, ultrasound imaging and diffuse optical imaging (DOI) were tested in the hope of constructing clinically applicable devices and techniques in addition to X-ray mammography. MRI has the advantage of providing a three-dimensional view of the breast, performing with high sensitivity in dense breast tissue and non-ionizing radiation while its high cost appears to be an important disadvantage (7). Ultrasound imaging has large penetration depth while it is limited by poor contrast and speckle problems (8-10).

Diffuse optical imaging for breast lesion detection was first used in 1929 (11). Advancement of laser and detection technologies has led to the application of Near-IR (NIR) lasers for Diffuse optical imaging (DOI). Diffuse optical imaging, and particularly NIR-DOI, unlike conventional X-ray mammography is non-ionizing since the light used in this method has much longer wavelength than X-ray. Moreover, it is noninvasive as there is no need to extract biopsies.

Diffuse optical imaging technique is based on the detection of light after propagation in tissue. Passing a biological tissue, light is both scattered and absorbed. The number of absorption events per unit length is referred to as absorption coefficient, $\mu_a$. Oxyhemoglobin, HbO, and dioxyhemoglobin, HHb, are the dominant organelles responsible for light absorption. The number of scattering events per unit length is referred to as scattering coefficient, $\mu_s$. For most biological tissues, the scattering coefficient is much larger than the absorption coefficient (12), in other words, light is diffused while propagating in biological tissues. Another important parameter in investigation of light propagation in diffusive media is the anisotropic factor, g, which is the average of the scattering angles. It has a value between -1 and 1, representing backward and forward scattering, respectively. If g = 0 the medium is isotropic. It is common in the literature to describe the scattering properties of tissue via reduced scattering coefficient which is defined as follows:

$$\mu'_s = \mu_s (1 - g) \tag{1}$$

Lesion detection in diffuse optical imaging is based on the difference in absorbing and scattering properties of healthy and cancerous tissue. In 2001, Gosh showed that the scattering and absorbing coefficients of healthy and cancerous breast tissue are different for visible light (13). Later in 2006 it was shown by Salomatina that there is a substantial difference in absorbing and scattering coefficients of healthy and cancerous breast tissue for NIR light (14).

To measure the intensity of light after propagation in a biological medium, light should be collected by a detector and the data achieved has to be processed by computer programs. There are two approaches for the detection of light in diffuse optical imaging; translumination, in which the source and detector are placed at opposite sides of the sample, and tomography, in which source and detector are placed over the surface and the detector or the source might scan the sample or there might be more than one source or detector sending or collecting light in various spatial positions. The more the number of source and detection fibers are, the larger number of spatial positions can be studied. Therefore, it is common amongst optical tomography devices to have large numbers of optical fibers placed in different positions (15-17). Nevertheless, it is also possible to use one optical fiber as the source fiber and one optical fiber as the detection fiber and have one or both of the fibers orbited around the sample to provide information for several spatial positions.

Due to low-cost and small size of laser diode, in our optical tomography device, NIR light from a diode laser enters the sample. An optical fiber collects light exiting the outer boundaries of the phantom. This optical fiber is connected to the detector. In order to collect light from all around the phantom, this fiber orbits around it. The pattern of light's intensity arrived to the detector is processed by the computer and the graph of the intensity versus the detection angle is drawn. The shape of the graph is different for phantoms with different optical properties. Also, when there is a defect inside the phantom, for angular positions in the vicinity of that defect the pattern of light intensity diagram changes. Defects are materials with different optical properties from the original phantom. Additionally, the result obtained from the setup is compared to the results obtained by a numerical solution of diffusion equation which simulates the graph of light intensity for the same angels as the experimental setup. The numerical solution is an evidence for the correctness of the experiment. Moreover, the simulation can add to

the device's accuracy for detecting the position of the defect. The experiment provides a wider vicinity of the defect and the simulation provides the more accurate position. It was seen that the best match of the plots obtained for the light intensity was achieved when the position of the defect best matches for experiment and simulation

The study of accuracy and precession of a low-cost instrument for optical imaging is the main aim of this article. So, the obtained results and images of this instrument are compared with the results obtained by numerical finite element method (FEM).

## Methods

A diffuse optical imaging device is made in order to study the light transmitted or backscattered from samples. The samples are biological phantoms which are constructed in cylindrical shapes. Phantoms, which are placed inside the device, are illuminated by NIR light of a diode laser.

Construction of the phantoms:

Phantoms are made from intralipid and ink. These phantoms represent the optical properties of breast tissue. The absorption coefficient of ink is measured using Beer-Lambert law:

$$I(z) = I_0 \exp(-\mu_a z) \qquad (2)$$

$I_0$ is the initial intensity of light, $I(z)$ is the light intensity z units of length after entering the medium.

The scattering coefficient of intralipid is derived from the following equations: (16)

$$\mu_s = 2.54 \times 10^9 \times \lambda^{-2.4} \qquad (3)$$
$$g = 1.1 - (0.58 \times 10^{-3} \times \lambda) \qquad (4)$$

Experimental setup:

Laser Light-780 nm, approximately 20 mW- is brought to the phantom from a laser diode (WSTech, UT5-50G-780) by an optical fiber (Ocean Optics- QP-400-2-VIS/NIR). The position of this optical fiber is fixed.

The light which is passed through the phantom is collected by an optical fiber (Ocean Optics- QP-400-2-VIS/NIR). One side of this optical fiber orbits around the phantom so that it can collect data from different angles and the other part is connected to a detector (Femtowatt photoreceiver, silicon detector, 320-1100 nm, PDF10A).

When light passes a diffusive medium, part of it is diffusely reflected (backscattered) and part of it is diffusely transmitted. Since the fiber which collects the data orbits around the phantom, it collects both the backscattered and transmitted light. In order to clarify the meaning of the angles used in this article, they are defined as follows:

If we assume that the cylinder's circumference contains 360°. We consider that the origin is where the source fiber is placed. The detecting fiber orbits around the phantom in a counter-clockwise fashion. Therefore in this entire article, for example, 10° means 10° counter-clockwise from the source. Furthermore, in some parts of the experiment, defects with optical properties different from the original phantom are placed inside them. Therefore, when it is reported that the position of the defect inside the phantom is X degrees it means that the center of the defect is placed in the X degrees according to the aforementioned criterion. It is worth mentioning that while the detecting fiber is placed in 0-90° and 270-360° (counter clockwise) it collects the backscattered light and when it is placed in 90-270° it collects the diffusely transmitted light.

A data acquisition card (Advantech, PCI-1714), which collects the analog data and converts it to digital, is used to relate the detector with the computer.

The phantom and the detecting optical fiber are set on a step motor. The step motor has steps of 2 degrees and covers 360° in 180 steps. Nevertheless, data are collected every four steps. Therefore the data are collected every 8 degrees. The backscattered light's intensities in angular positions between 0-40 degrees and 320-360 are considerably larger than the other parts and cause limitations for data processing; therefore the detector's movement starts from 40 degrees and ends in 320 degrees. Consequently, data are collected in 35 steps. Controlling of the step motor's movement and data processing is performed via LabVIEW software package. It is also programmed so that in any collecting step, data is received 30 times and the average value is saved. The average values have been used in the diagrams representing the results.

A schematic of the setup is depicted in figure 1.

## Results and discussion

### A. Homogenous healthy breast tissue

Phantoms with optical properties close to healthy breast tissue were constructed. The diagrams of the diffused light's intensity in different angles were
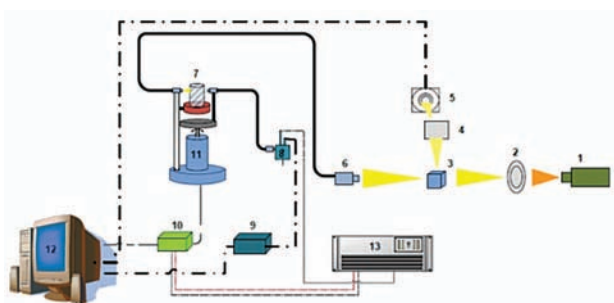
**Figure 1.** The schematic of the setup. Light from laser diode (1) passes a polarizer (2), which is used for changing the power of light. Then it is divided into two parts by a beam splitter (3). One part is used as a reference light after passing a filter (4). The reference light is detected by a detector (5). The other part enters an optical fiber (6) and enters the phantom (7). Then it is sent to the main detector (8) by another optical fiber of the same kind. In order to avoid losing data a voltage reducer (9) is used before the data is sent to the PC (12). The detecting optical fiber is orbited around the phantom by a stepper motor (11) which is controlled by the stepper motor driver (10). The electrical power of the whole system is supplied by a power supply (13).

plotted using the achieved data.

Two phantoms were constructed with different reduced scattering coefficients but equal absorption coefficients. The first phantom's reduced scattering coefficient was 16 $cm^{-1}$ and the second phantom's reduced scattering was 27 $cm^{-1}$. They both have an absorption coefficient of 0.05 $cm^{-1}$.

Results achieved experimentally and numerically are compared with each other and a good correlation is observed. The correlation coefficient is defined as a measure of linear association between two variables and as it approaches 1 and -1 it shows stronger association. The square of correlation coefficient is called the coefficient of determination $R^2$. The value of $R^2$ between numerical and experimental results equals 0.999 for the first phantom and 0.995 for the second phantom.

### B. Healthy breast tissue with lesion inside

Phantoms with cylindrical defects inside them were constructed. In one experiment, phantoms with optical properties close to healthy breast tissue were constructed and smaller empty cylinders were excavated in them (air defect) and in another experiment there were cylinders with optical properties close to tumorous breast tissue placed inside the phantoms in different positions (tumorous defect). Experiments were carried out for these phantoms and the diagrams were plotted. The same situation was simulated by FEM code and the resulting diagrams were compared with the experimental diagrams.

### B-1. Air defect

In the experiment carried out with air defect, the center of the defect is placed 13 mm from the inner wall of the original cylinder and it has a diameter of 7 mm. Its angular position is 90 degrees with respect to the incident light. The diagram for this phantom was plotted and when it was fitted to a diagram obtained by FEM, $R^2$ was 0.9993224. The fractional error for the diameter was 14.2% and the fractional error for the position of the center was 7.6%. The diagrams are depicted in figure 2.

### B-2. Tumorous defect

Three phantoms were constructed in which the defect had the optical properties of tumorous breast tissue.

In one experiment the center of the defect was placed 6 mm from the inner wall of the original cylinder and its diameter was 7 mm. The defect's angular position was 90 degrees with respect to the incident light. The reduced scattering and absorption coefficients of the healthy part were 18 and 0.05 $cm^{-1}$, respectively. The reduced scattering and absorption coefficients of the tumorous part were 30 and 0.5 $cm^{-1}$, respectively. $R^2$ between the experimental and simulated diagrams was 0.995146. The fractional error for the position of the center of the circle was found to be 13.33% and the fractional error for the diameter of the defect was
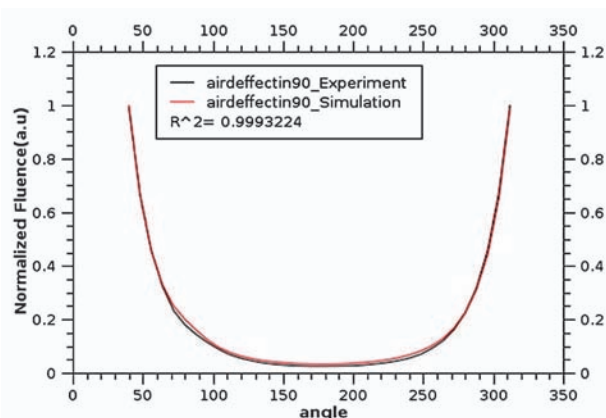


**Figure 2.** The red plot is obtained by finite element simulation with air defect with diameter of 8 mm. The defect is placed in 90 degrees and 12 mm depth. The black plot is the experimental data for the phantom with the same properties. The defect is placed 13 mm deep and has a diameter of 7 mm. Therefore, FEM code has a fractional error of 7.6% and 14.2% for the depth and the diameter of the defect, respectively. In the vicinity of 90 degrees the value of light intensity is slightly increased since there was no absorbing and scattering material in that position.

found to be 31.42%. The experimental and simulated diagrams are depicted in figure 3,4.

In another experiment the defect was placed in the angular position of 180 degrees with respect to the incident light. Its diameter was 7 mm and its center was 6 mm from the inner wall of the original cylinder. The reduced scattering and absorption coefficients of the healthy part were 14 and 0.05 $cm^{-1}$, respectively. The reduced scattering and absorption coefficients of the tumorous part were 35 and 1 $cm^{-1}$, respectively. The fractional error for the position of the center of the defect was 1.67% and the fractional error for

the diameter of the defect was 8.57 %. $R^2$ between the experimental and the simulated diagrams was 0.9966428. The two diagrams are plotted in figure 5,6.

Lastly, a tumorous defect was positioned in the angular position of 270 degrees. Its diameter was 7 mm and its center was positioned 6 mm from the inner wall of the original cylinder. The reduced scattering and absorption coefficients of the healthy part were 18 and 0.05 $cm^{-1}$, respectively. The reduced scattering and absorption coefficients of the tumorous part were 25 and 0.2 $cm^{-1}$, respectively. The fractional error
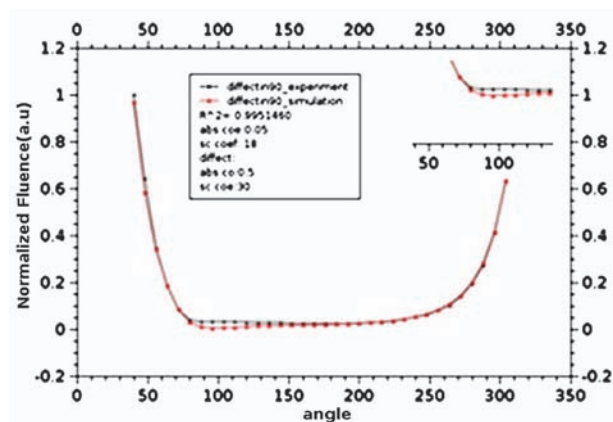


**Figure 3.** The red curve is the simulated graph obtained by the FEM code and the black curve shows the experimental graph. The defect is placed in 90 degrees. It is clear from the figure that the intensity of the detected light is decreased in the vicinity of 90 degrees (as highlighted in the top right corner of the figure). The diameter of the defect is 7mm and the center of the circle is 6mm from the inner wall of the container, while in the FEM code they are predicted to be 9.2 mm and 5.2 mm, respectively.
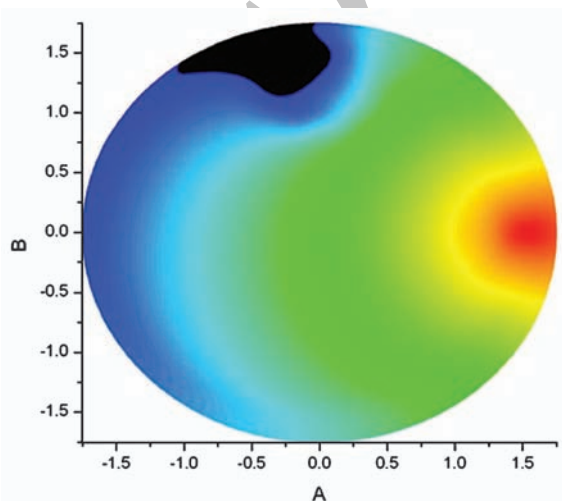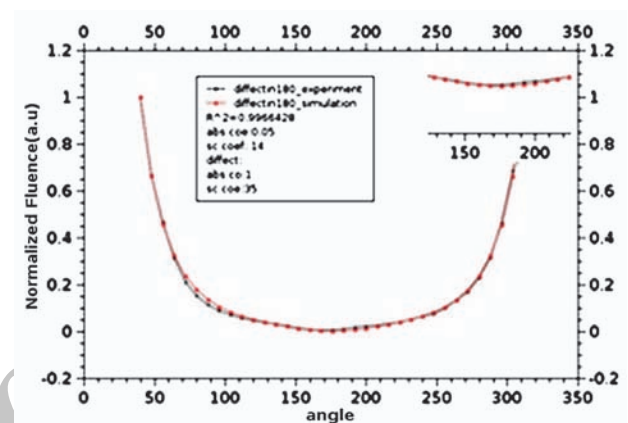


**Figure 5.** The red curve is the simulated graph obtained by the FEM code and the black curve shows the experimental graph. The defect is placed in 180 degrees. It is clear from the figure that the intensity of the detected light is decreased in the vicinity of 180 degrees (as highlighted in the top right corner of the figure). The diameter of the defect is 7mm and the center of the circle is 6mm from the inner wall of the container, while In the FEM code the position of the center of the circle is assumed to be 6.1 and the diameter of the circle is assumed to be 7.6mm.
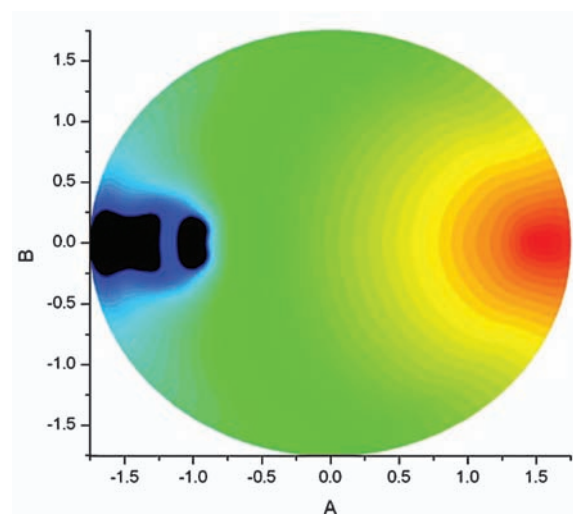


**Figure 4.** A schematic of the defect inside the phantom. The defect, which is represented by dark color, is placed in 90 degrees as defined by the criterion mentioned in materials and methods section.



**Figure 6.** The position of the defect is 180 degrees regarding the aforementioned criterion. The dark section represents the phantom. The red part represents the source.

for the position of the center of the defect was 15% and the fractional error for the diameter of the defect was 8.5%. The coefficient of determination between the experimental and the simulated diagrams was 0.9947946. The experimental and simulated diagrams are depicted in figure 7,8.

Conclusively the data derived for tumor detection in this study is summarized in table 1. The results indicate that this tomography device is capable of detecting defects inside phantoms. The fractional errors are caused by the accuracy of FEM's mesh formation.

## Conclusion

In this study a low-cost optical tomography device is made. Biological phantoms are constructed and are used as samples in optical tomography. The data achieved by the optical tomography device is compared with the data achieved via a FEM code written in FORTRAN. Phantoms with defects inside are constructed and the ability of the constructed device in finding the diameter and the position of the center of defects is assessed. Fractional errors in lesion detection are due to inaccuracy of the FEM's mesh formation and the device. The results indicate that the presented device is capable of providing the correct pattern of diffusely backscattered and transmitted light. Lesion detection has also been performed via the device. The data achieved from the device is in excellent correlation with the numerical solution of the diffusion equation in cylindrical coordinates. It is worth mentioning that in many optical tomography devices, the place of the source fiber is switched so that light enters the medium from various locations according to the lesion in order to provide reliable information while in our setup the source fiber's position is fixed. It is noticed that reliable data is achieved for lesions which are far from the source (B-2, 180 degrees). Care has been taken to align the fibers very carefully and the experiment has been carried out for several phantoms and lesions in several locations. Therefore, results indicate the applicability of the reported device. This device may be used as a base for an optical imaging system.
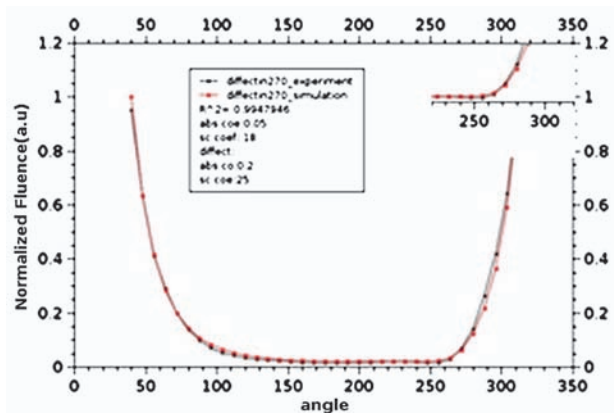


**Figure 7.** The red curve is the simulated graph obtained by the FEM code and the black curve shows the experimental graph. The defect is placed in 270 degrees. It is clear from the figure that the intensity of the detected light is decreased in the vicinity of 270 degrees (as highlighted in the top right corner of the figure). The diameter of the defect is 7mm and the center of the circle is 6mm from the inner wall of the container, while in the FEM code the position of the center and the diameter of the circle re assumed to be 5.1mm and 7.6mm, respectively.
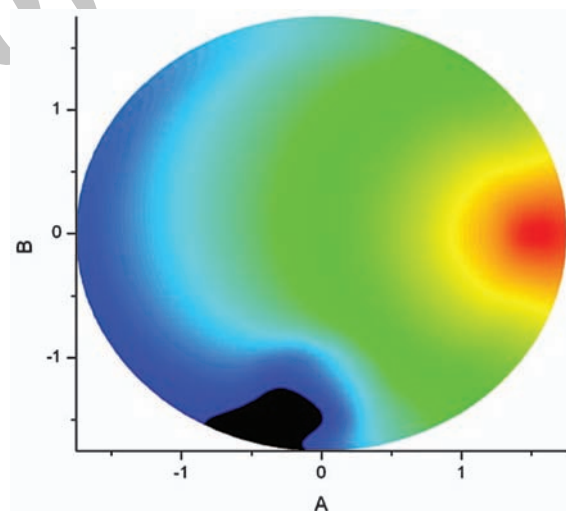


**Figure 8.** The dark part represents the defect and the red part represents the source. The defect is placed 270 degrees from the source.

**Table 1.** Summary of lesion detection results

| Type of defect | $\mu_a$ of healthy part (cm⁻¹) | $\mu'_s$ of healthy part (cm⁻¹) | $\mu_a$ of defect (cm⁻¹) | $\mu'_s$ of defect (cm⁻¹) | Angular position of defect (degrees) | Diameter of defect (mm) | Position of the center of defect (mm) | Fractional error for diameter of defect % | Fractional error for position of the center of defect % |
|---|---|---|---|---|---|---|---|---|---|
| Air | 0.05 | 16 | 0 | 0 | 90 | 7 | 13 | 14.2 | 7.6 |
| Tumor | 0.05 | 18 | 0.5 | 30 | 90 | 7 | 6 | 31.42 | 13.33 |
| Tumor | 0.05 | 14 | 1 | 35 | 180 | 7 | 6 | 8.57 | 1.67 |
| Tumor | 0.05 | 18 | 0.2 | 25 | 270 | 7 | 6 | 8.5 | 15 |

# References

1. The cancer cure foundation [Internet].California:The fondation; C2002-2012, Available from http://www.cancure.org/statistics.htm

2. Breast cancer: incidence rises while death continues to fall. Available via http://www.statistics.gov.uk. Dec 2006

3. Tabar L, Yen MF, Vitak B, Chen HH, Smith RA, Duffy SW. Mammography service screening and mortality in breast cancer patients: 20-year follow-up before and after introduction of screening. Lancet 2003; 361(9367):1405-10.

4. Huynh PT, Jarolimek AM, Daye S. The false-negative mammogram. Radiographics 1998; 18(5):1137-54.

5. Elmore JG, Barton MB, Moceri VM, Polk S, Arena PJ, Fletcher SW. Ten-year risk of false positive screening mammograms and clinical breast examinations. N Engl J Med 1998; 338(16):1089-96.

6. Lucassen A, Watson E, Eccles D. Evidence based case report: Advice about mammography for a young woman with a family history of breast cancer. BMJ 2001; 322(7293):1040-2.

7. Hylton N. Magnetic resonance imaging of the breast: Opportunities to improve breast cancer management. J Clin Oncol 2005; 23(8):1678-84.

8. Wang X, Pang Y, Ku G, Xie X, Stoica G Wang LV. Non-invasive laser-induced photoacoustic tomography for structural and functional imaging of the brain in vivo. Nat Biotechnol 2003; 21(7): 803-6.

9. Su Y, Zhang F, Xu1 K, Yao J, Wang RK. A photoacoustic tomography system for imaging of biological tissues. J Phys D: Appl Phys 2005; 38 (15): 2640-4.

10. Tokuno H, Hatanaka N, Takada M, Nambu A. B-mode and color Doppler ultrasound imaging for localization of microelectrode in monkey brain. Neurosci Res 2000; 36(4):335-8.

11. Cutler M. Transillumination of the breast. Surg Gynaecol Obstet 1929; 48:721-7.

12. V.V Tuchin(ed), Handbook of photonics for biomedical science. CRC Press. Boca Raton. 2010.

13. Ansari MA, Alikhani S, Mohajerani E, Massudi R, The numerical and experimental study of photon diffusion inside biological tissue using boundary integral method, Opt Commun 2012; 285(5):851-855.

14. Salomatina E, Jiang B, Novak J, Yaroslavsky AN. Optical properties of normal and cancerous human skin in the visible and near infrared spectral range. J Biomed Opt 2006;11(6): 064026.

15. Iftimia N, Gu X, Xu Y, Jiang H. A compact parallel-detection optical mammography system. Rev Sci Instrum 2003; 74:2836-42.

16. Choe R. Diffuse optical tomography and spectroscopy of breast cancer and fetal brain, p. 83. Thesis of doctor of philosophy, Department of Physics and Astronomy University of Pennsylvania, 2005.

17. Yang J, Zhang T, Yang H, Jiang H, Fast multispectral diffuse optical tomography system for in vivo three-dimensional imaging of seizure dynamics, Appl Optics 2012; 51(6): 3461-3469.